Volume 1 | Number 1 | Jan 2013 | Pages 1–100

PCCP

Physical Chemistry Chemical Physics
www.rsc.org/pccp

ROYAL SOCIETY OF CHEMISTRY

This is an *Accepted Manuscript*, which has been through the Royal Society of Chemistry peer review process and has been accepted for publication.

Accepted Manuscripts are published online shortly after acceptance, before technical editing, formatting and proof reading. Using this free service, authors can make their results available to the community, in citable form, before we publish the edited article. We will replace this *Accepted Manuscript* with the edited and formatted *Advance Article* as soon as it is available.

You can find more information about *Accepted Manuscripts* in the **Information for Authors**.

Please note that technical editing may introduce minor changes to the text and/or graphics, which may alter content. The journal's standard **Terms & Conditions** and the **Ethical guidelines** still apply. In no event shall the Royal Society of Chemistry be held responsible for any errors or omissions in this *Accepted Manuscript* or any consequences arising from the use of any information it contains.

ROYAL SOCIETY OF CHEMISTRY

www.rsc.org/pccp

Physical Chemistry Chemical Physics

PAPER

Revealing the structure−property relationships of covalent organic frameworks for CO_2 capture from postcombustion gas: a multi-scale computational study

Minman Tong, Qingyuan Yang*, Yuanlong Xiao and Chongli Zhong*

Abstract

With the aid of multi-scale computational methods, a diverse set of 46 covalent organic frameworks (COFs), covering most typical COFs synthesized up to date, were collected to study the structure-
10 property relationships of COFs for CO_2 capture. For this purpose, CO_2 capture from postcombustion gas (CO_2/N_2 mixture) under industrial vacuum swing adsorption (VSA) conditions was considered as an example. This work shows that adsorption selectivity, CO_2 working capacity and sorbent selection parameter of COFs all exhibit strong correlation with the difference of the adsorbility of adsorbates (ΔAD), highlighting that realization of large ΔAD can be regarded as an important starting point for
15 designing COFs with improved separation performance. Furthermore, it was revealed that the separation performance of 2D-layered COFs can be greatly enhanced by generating "splint effects", which can be achieved through structural realignment to form slit-like pores with suitable size in the structures. Such "splint effects" in 2D-COFs can find its similar counterpart of "catenation effects" in 3D-COFs or MOFs. On the basis of these observations, a new design strategy was proposed to strengthen the separation
20 performance of COFs. It could be expected that the information obtained in this work not only will enrich the knowledge of the structure-property relationships of COFs for separation, but also will largely facilitate their future applications to the fields related to energy and environmental science, such as natural gas purification, CO_2, NO_x and SO_x capture, etc.

1. Introduction

25 In the transition toward a more sustainable energy economy, carbon-based fuels still remain the dominant role in worldwide energy supply for the foreseeable future. However, the excessively anthropogenic release of CO_2 to the atmosphere has triggered serious global climate issues.[1] Out of consideration for
30 environmental protection, it is thus an urgent task to search feasible technologies with minimal environmental impact and low costs for removing this greenhouse gas from various gas streams or flue exhaust. The current commercial chemical absorption methods using aqueous amine solutions for carbon
35 capture and sequestration (CCS) bear several drawbacks such as corrosion control and high energy penalty needed for the solvent regeneration.[2] In contrast, pressure or vacuum swing adsorption (PSA or VSA) process on the basis of porous solids provides a promising alternative for this target.[3] Up to date, significant
40 efforts have been conducted to evaluate the feasibilities of various materials, including activated carbons, zeolites and metal-organic frameworks (MOFs), and plentiful suggestions have been

brought out to improve their performance on CO_2 capture.[4-11] Currently, attentions are being paid to find new materials with
45 even better performance.

Covalent organic frameworks (COFs) represent a novel class of crystalline nanoporous materials in which organic building units are assembled together to form periodic networks *via* strong covalent bonds.[12] The highly-ordered architectures of such
50 intriguing materials possess many fascinating features like low framework density, tuneable porosity, high thermal stability and easy chemical functionalization.[13,14] Since the landmark work of Yaghi and co-workers in 2005,[12] the rapid growth in the community of COFs has attracted intensive attention of
55 researchers coming from different fields. Several excellent reviews have been published on summarizing the development in design, synthesis, characterization and application studies of COF-type materials.[13-16] The existing studies have demonstrated that some COFs can exhibit promising properties for CO_2
60 capture.[17-20] Additionally, chemically and water stable COFs are increasingly reported in the literature,[19-25] which is one of the vital prerequisites related to the practical utility of such materials.

At the moment, the studies for COFs are mainly focused on the discovery of new structures,[26-28] while those on revealing the structure−property relationships of COFs for a certain practical application are very scarce,[29] especially with regard to CO_2 capture. However, such studies are crucial for enabling a theoretically rapid screening of COFs as well as for guiding the design and synthesis of new COFs with improved performance.

Motivated by the context described above, a multi-scale computational study was conducted in this work to investigate the structure-property relationships of COFs for CO_2 capture. The removal of CO_2 from postcombustion gas (CO_2/N_2 mixture) *via* VSA process was selected as an example for case study. The bulk composition of the mixture was taken as $CO_2:N_2 = 15:85$, and the operating pressures were 1 bar for adsorption and 0.1 bar for regeneration, corresponding to the typical concentration of flue gas emitted from power plants and the industrial VSA conditions for separating this system.[30] More particularly, attention was paid, for the first time, on studying the influence of the distinctive layered characteristics of two-dimensional (2D) COFs on separation. Following the structure-property relationships established in this work, a new strategy was further proposed for tuning/designing COFs with improved performance for CO_2 capture. The information obtained not only can enrich the knowledge of gas separation performance of COFs, but also may be beneficial to a better understanding of the structure-property relationships of other nanoporous materials.

2. Models and computational methods

2.1 COF structures

To obtain reliable structure-property relationships of COFs for a targeted application, it is crucial to have a representative structural database. In current work, a diverse set of 46 typical COFs were collected from literature, covering the most well-known subfamilies and newly synthesized materials reported up to date. All the framework structures were constructed from the data published in their corresponding synthetic studies. In this relatively large database, there are 2D-COFs with hexagonal and tetragonal topologies and 3D-COFs with **ctn, bor** and **dia** topologies; from a perspective of chemical compositions, the structures involve almost all of the main group light elements that are composed of COF-type materials synthesized so far (C, O, B, N, H, F, Si, etc.), as well as some heavy metals (like Zn and Ni) that present in some cases on the porphyrin-like rings of several materials. By examining the organic building units, there are diverse species including porphyrin, pyrene, triazine, cyclotricatechylene (CTC), 1,3,5-tris(4-formyl)benzene, hexahydroxytriphenylene (HHTP), and 1,3,5-triformylbenzene, etc. In terms of structural series, there are boron-COFs, imine-COFs, CTFs, Tp-COFs, NPNs, Star-COFs, BLP, and CTC, etc. Their structural properties like accessible surface area, pore size and porosity span a wide range of values, as provided in Table S1 in the ESI†. Therefore, the 46 COFs selected carefully can represent the existing COFs quite comprehensively, which provides a solid basis for obtaining general and reliable results.

2.2 Quantum mechanical calculations

To model guest-host intermolecular interactions more rigorously, the electrostatic contributions were also taken into account in this

study. For this purpose, assigning atomic partial charges can be regarded as a convenient and good compromise between computational effectiveness and accuracy. Therefore, quantum mechanical (QM) approach on the basis of density functional theory (DFT) was performed on the clusters cleaved from the unit cell of each selected COF structure. Since the terminations of the cleaved model clusters are all connected with organic linkers, they were saturated by methyl groups with standard sp^3 geometry. The electrostatic potential (ESP) charges obtained with the grid-based ChelpG algorithm were used as the atomic partial charges, which has been recognized as one of the most popular and reliable electrostatic charge calculation methods.[31-33] All DFT calculations were accomplished with the GAUSSIAN03 software [34] using the Becke plus Lee-Yang-Parr (B3LYP) functional. The all-electron basis set 6-31+G* was used for the framework atoms of light elements which includes one diffuse and one polarization function on atoms heavier than He. For heavy atoms, effective core potential (ECP) is often chosen in QM calculations to reduce the amount of the necessary computation. LANL2DZ is a collection of double-ζ basis sets, which is one of the most common ECP basis sets for complexes involving transition metal elements. Thus, this basis set was adopted for the heavy atoms Zn and Ni in the COFs. The above set of computational methods has been widely adopted to calculate the atomic partial charges for MOFs[35] and COFs.[32,36,37] The model clusters adopted in this work for the 46 COFs and their atomic partial charges are given in the ESI† (Fig. S1-45)

To compare the influences of the electrostatic properties of some COFs of interest on CO_2/N_2 separation, periodic DFT calculations were performed to extract the electrostatic potential distributions in the unit cells of the materials. The calculations were performed using the Dmol^3 module implemented in the Materials Studio software,[38] where the PW91 GGA functional combined with the double numerical basis set containing polarization function on hydrogen atoms (DNP) were employed. Such an approach has been successfully utilized to analyze the physicochemical properties of MOFs and COFs.[35,39]

2.3 Force fields

In present work, a combination of the site-site Lennard-Jones (LJ) and Coulombic potentials was employed to calculate the intermolecular interactions between adsorbates and adsorbates as well as between adsorbates and COFs. CO_2 was modelled as a rigid linear molecule (C−O bond length of 1.149 Å) with three charged LJ interacting sites located on each atom. The LJ potential parameters for atom O ($\sigma_O = 3.033$ Å and $\varepsilon_O/k_B = 80.507$ K) and atom C ($\sigma_C = 2.757$ Å and $\varepsilon_C/k_B = 28.129$ K) were taken from the EPM2 force field developed by Harris and Yung.[40] Partial point charges centred at each LJ site are $q_O = -0.3256e$ and $q_C = 0.6512e$. N_2 was represented using the TraPPE force field reported by Potoff and Siepmann,[41] where two of the three charged sites are located at two N atoms and the third one is situated at its centre of mass (COM). The N–N bond length is 1.10 Å and only the N atoms are the LJ interacting sites ($\sigma_N = 3.31$ Å and $\varepsilon_N/k_B = 36.0$ K). Each N_2 molecule is assigned a negative charge on the N atoms ($q_N = -0.482e$) and a positive charge on the COM site ($q_{COM} = 0.964e$). The two potentials have been used to accurately reproduce the experimental vapour-liquid phase equilibrium data of each gas in the bulk states. An

atomistic representation was used for all the COFs studied in this work. The LJ potential parameters for the framework atoms of COFs were taken from the DREIDING force field,[42] and the missing parameters for the metal Ni were taken from the
5 Universal force field (UFF),[43] as given in Table S2 (see the ESI†).

The Lorentz−Berthelot mixing rules were used to determine all of the LJ cross potential parameters between adsorbate−adsorbate and adsorbate−COF interactions. The above set of force fields has been widely used for describing the adsorption of CO_2/N_2
10 mixture in MOFs.[35]

2.4 Simulation details

Grand canonical Monte Carlo (GCMC) simulations were employed to investigate the adsorption behaviours of CO_2/N_2 mixture in COFs at 298 K, using our in-house code CADSS
15 (Complex Adsorption and Diffusion Simulation Suite). During the simulations, molecules involve five types of trials: attempts (i) to randomly displace a molecule (translation or rotation), (ii) to regrow a molecule at a random position, (iii) to create a new molecule, (iv) to delete an existing molecule, and (v) to exchange
20 molecular identity. All of the COFs were treated as rigid frameworks with atoms frozen at their crystallographic positions, as usually done by others.[44] The numbers of the unit cells contained in the simulation box are COF-dependent, ranging from $1\times1\times9$ to $2\times2\times10$, and no finite-size effects existed by
25 checking the simulations with larger boxes. A cutoff distance was set to 14.0 Å for the LJ interactions, while the long-range electrostatic interactions were handled using the Ewald summation technique. Periodic boundary conditions were considered in all three dimensions. Peng-Robinson equation of
30 state was used to convert the pressure to the corresponding fugacity used in the GCMC simulations. For each state point, GCMC simulations consisted of 2×10^7 steps to ensure the equilibration, followed by 2×10^7 steps to sample the desired thermodynamic properties. For the calculation of the isosteric
35 heat of adsorption (Q_{st}^0) for CO_2 and N_2 at the limit of zero-coverage, configurational-bias Monte Carlo (CBMC) simulations in the canonical (NVT) ensemble were performed using the revised Widom's test particle method.[45]

2.5 Property calculations

40 The following four evaluation criteria [46], as adopted commonly in previous work, were used to study the structure-property relationships of the COFs in our database for CO_2/N_2 separation.

The selectivity (S_{CO_2/N_2}) of CO_2 over N_2 under adsorption conditions is defined by

$$S_{CO_2/N_2} = (x_{CO_2}/x_{N_2})(y_{N_2}/y_{CO_2}), \quad (1)$$

45 where x and y are the mole fractions of the two gases in the adsorbed and bulk phases, respectively.

The working capacity (ΔN_{CO_2}) of the targeted component CO_2 is described by the difference between the amounts of the gas in the adsorbed mixture at the corresponding adsorption
50 ($N_{CO_2}^{ads}$) and desorption ($N_{CO_2}^{des}$) conditions, in units of mol gas per kg of adsorbent

$$\Delta N_{CO_2} = N_{CO_2}^{ads} - N_{CO_2}^{des} \quad (2)$$

The Sorbent selection parameter (S_{sp}) that can characterize the total separation efficiency is defined as

$$S_{sp} = \frac{\left(S_{CO_2/N_2}^{ads}\right)^2}{S_{CO_2/N_2}^{des}} \times \frac{\Delta N_{CO_2}}{\Delta N_{N_2}} \quad (3)$$

where S_{CO_2/N_2}^{des} is the selectivity at the desorption conditions, and
55 ΔN_{N_2} is the working capacity of the component N_2.

Regenerability (R) is also an important parameter to evaluate the practical usefulness of an adsorbent for cyclic PSA and VSA processes, which is defined as the ratio of the working capacity of CO_2 to its adsorbed amount at the adsorption conditions.

$$R = \left(\Delta N_{CO_2}/N_{CO_2}^{ads}\right) \times 100\% \quad (4)$$

60 ## 3. Results and discussion

3.1 Atomic partial charges in COFs

Atomic partial charges are usually required in the molecular simulations for studying the separation of CO_2-containing gas mixtures in adsorbents. Consequently, they are firstly calculated
65 for the 46 COFs using the DFT methods described previously. Fig. 1 shows the model clusters and the obtained atomic partial charges for some typical COFs, while the corresponding results for the rest of materials are shown in the ESI†.

70
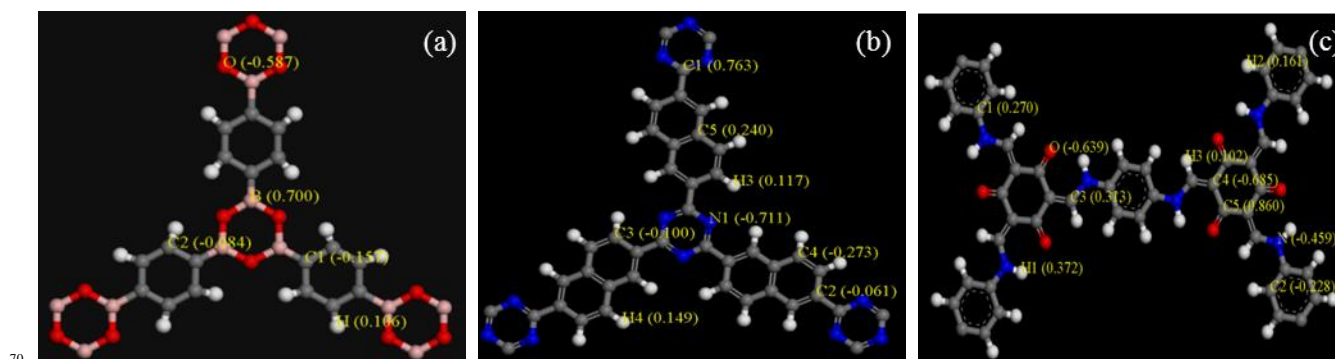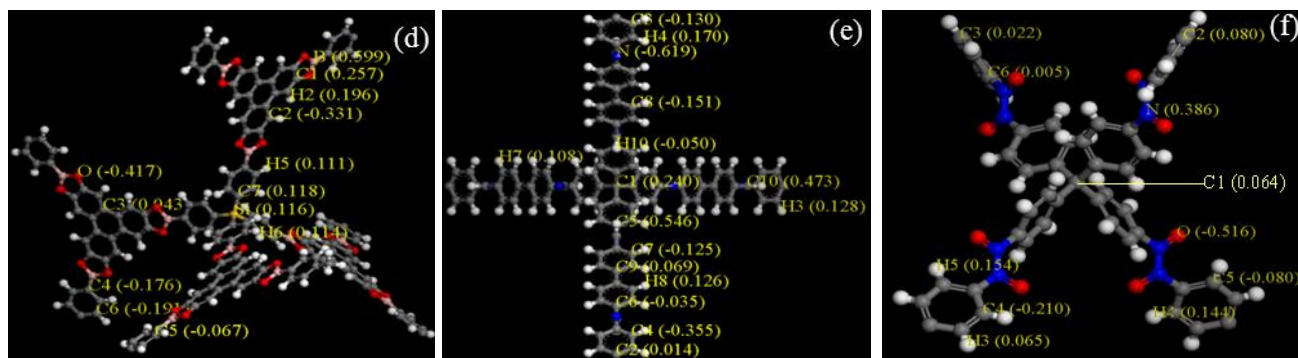
Fig. 1 Model clusters and the DFT-derived atom partial charges of some typical COFs: (a) COF-1, (b) CTF-2, (c) TpPa-1, (d) COF-105, (e) COF-320 and (f) NPN-1. For clarity, the methyl groups used for saturating the clusters are omitted (B: pink; O, red; C, gray; N, blue; S, yellow; H, white).

3.2 Establishment of structure-separation performance relationships of COFs

Since structure-property relationships are crucial for rational design of COFs for a certain application, we first make an effort to establish the relationships between the separation properties (selectivity, working capacity and sorbent selection parameter) of COFs with the physicochemical properties of the materials. Therefore, GCMC simulations were carried out to calculate the properties to be studied, then efforts were made to find the relationships between them. Details are given in the following paragraphs.

3.2.1 Structure-selectivity relationships

The selectivity perhaps is the key evaluation criterion that is most commonly used to compare the separation performance of different adsorbents. Thus, on the basis of a single-factor analysis method, we began with examining the relationships between this parameter and some relevant descriptors that characterize the structural features of the adsorbents, including the specific accessible surface area (S_{acc}), free volume (V_{free}) and porosity (φ). Figs. 2a-c show the dependence of the simulated CO_2/N_2 adsorption selectivity of the 46 COFs at 298 K and 1 bar on these descriptors, respectively. As can be seen from these figures, selectivity does not show strong correlation with them.

The isosteric heat of adsorption at infinite dilution (Q_{st}^0) is an important energetic factor that is usually used to describe the intrinsic adsorption affinity of host structures with guest molecules. To characterize the separation performance of adsorbents, it has been demonstrated that the difference of this factor (ΔQ_{st}^0) between the two components in a mixture should be used instead of only that of the more strongly adsorbed component.[47] Considering this fact, we further examined the relationship of the selectivity with the ΔQ_{st}^0 between CO_2 and N_2,

as illustrated in Fig. 2d. Compared to the results shown in Figs. 2a-c, one can readily observe that the selectivity is more intimately associated with ΔQ_{st}^0, although the relationship is still not good enough.

The results in Figs. 2a-d demonstrate that selectivity does not correlate strongly with the commonly used single structural parameters, which should be affected by the interplay of two or more parameters. In our previous work, a concept named "adsorbility (AD)" was proposed for MOFs,[47] and good correlations between selectivity and the difference of adsorbility of adsorbates ($\Delta AD = \Delta Q_{st}^0/\varphi$) were found for MOFs.[10, 47] Very recently, this concept was successfully extended to porous polymers by Colina and coworkers,[48] encouraging us to see whether this concept is also applicable to COFs. The results in Fig. 2e show that much better correlation was obtained between selectivity and ΔAD, as compared to those with other parameters. Generally speaking, selectivity increases with increasing ΔAD; the good correlation makes ΔAD a valuable indicator for selectivity, that is, designing of COFs with large ΔAD can benefit to improve the separation selectivity.

3.2.2 Structure-working capacity relationships

One of the largest contributors to the capital and operating costs for CO_2 capture is the cost for the adsorbent and the large volume of the adsorber vessels required. In practice, the CO_2 working capacity of a material, instead of the absolute adsorption amount, is preferred to be used for evaluating its performance in a cyclic PSA or VSA process. Reduction in capital cost can be reached by using robust adsorbents with both high adsorption selectivity and working capacity. Thus, it is necessary to establish the relationships of working capacity with the physicochemical properties of COFs for postcombustion CO_2 capture using VSA process.
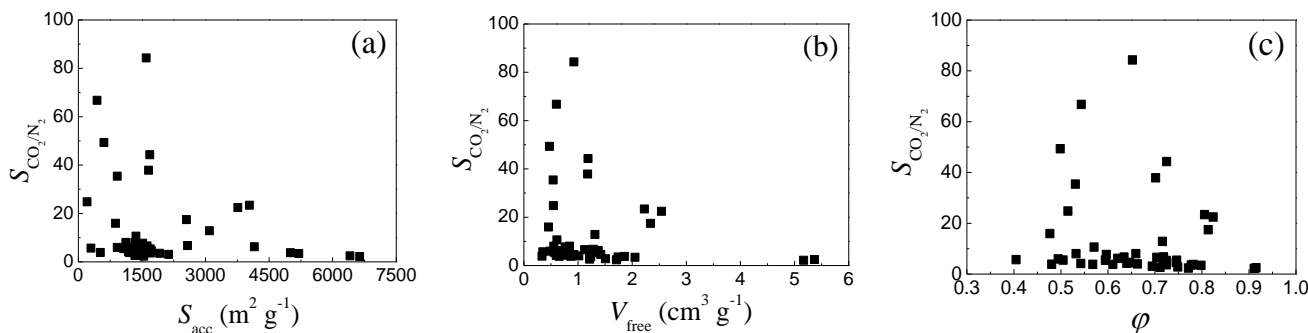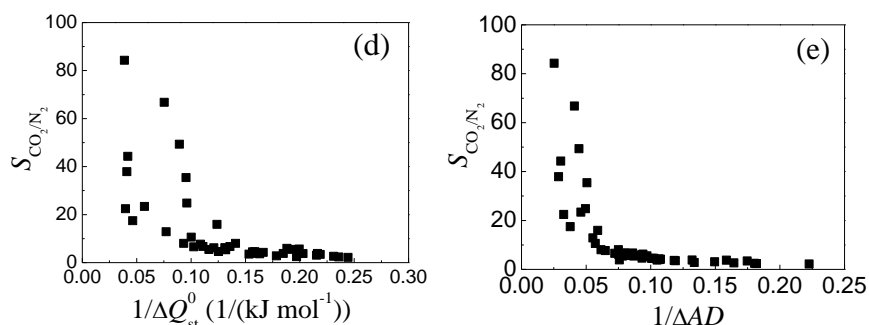
Fig. 2 Relationships between CO_2/N_2 adsorption selectivity and (a) specific accessible surface area (S_{acc}), (b) free volume (V_{free}), (c) porosity (φ), (d) difference of isosteric heat of adsorption between CO_2 and N_2 at infinite dilutions (ΔQ_{st}^0) and (e) difference of adsorbility between the two components (ΔAD). The bulk composition for the gas mixture is CO_2:N_2 = 15:85.

In light of the results shown in Fig. 2, attentions were paid to investigate the relationships between the CO_2 working capacity of the COFs with ΔQ_{st}^0 and ΔAD. As can be found from Fig. 3, the correlation between ΔN_{CO_2} and ΔQ_{st}^0 is highly scattered, while a good correlation exists for ΔAD. It has been found in many studies that the presence of strong CO_2 adsorption sites can contribute to the separation performance of a material.[35] However, Fig. 3a shows that some COFs have much higher ΔQ_{st}^0 than other materials but have relatively lower working capacity. By an examination of the structures of such materials, including TpPa-1,[22] TpBD,[23] DAAQ-TFP COF,[25] IL-COF-1,[18] COF-43[21] and COF-366,[49] it was found they not only contain strong CO_2 adsorption sites but also have large free volume/pore size (see Table S1 in the ESI†). These observations indicate that the density of strong adsorption sites in these materials is lower and thus ΔQ_{st}^0 is not sufficient to characterize their CO_2 working capacity. For a better understanding, we further analyzed the COM probability distributions of the adsorbed CO_2 molecules in the COFs at 1 bar and 298 K, for which the results in two typical materials of COF-366 and NPN-1 (corresponding to the points enclosed in the red and blue circles, respectively; see Fig. 3) were selected as examples, as shown in Fig. 4. The former has a 2D-layered structure with square pores (~20 Å) and each layer contains tetra(p-amino-phenyl) porphyrin bonded with a terephthaldehyde chain to form the periodic framework. The latter has a 3D four-fold interpenetrated structure in which the diamondoid networks are assembled together by the *trans*-azodioxy linkages to form channel-like pores with dimensions of 7.3×3.3 Å.[28] As can be seen from Fig. 4a, CO_2 molecules are mainly adsorbed between the consecutive porphyrin units of COF-366 and almost no CO_2 can be found in the square pores under the conditions considered. This means that although COF-366 has a high ΔQ_{st}^0 value (17.5 kJ mol^{-1}), the preferential adsorption sites (porphyrin units) for CO_2 are scarce in its large pore space, leading to a moderate CO_2 working capacity (see Fig. 3a). In contrast, Fig. 4b discloses that the channel-like micropores in NPN-1 provide suitable adsorption sites for CO_2, and the very dense adsorption sites result in the highest working capacity among the 46 COFs although the ΔQ_{st}^0 (11.2 kJ mol^{-1}) of the material is not the highest. These observations reveal the importance of combining both ΔQ_{st}^0 and density of adsorption
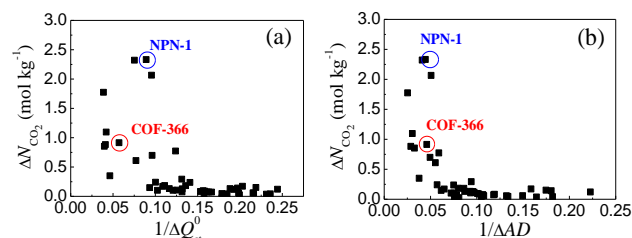
Fig. 3 Relationships between the working capacity and (a) ΔQ_{st}^0 and (b) ΔAD for CO_2/N_2 separation in the 46 COFs using VSA process

sites in predicting the working capacity of a material. As described elsewhere,[35] the physical meaning of adsorbility can be considered as a measure of the adsorption energy density for a gas in a given porous solid; it could be rationalized that an intimate correlation should exist between ΔAD and working capacity, as shown in Fig. 3b. In addition, a trend reflected from this figure is that materials with ΔAD larger than 20 (*i.e.*, $1/\Delta AD$ smaller than 0.05) are expected to have much greater probability for achieving better performance in regard of working capacity.
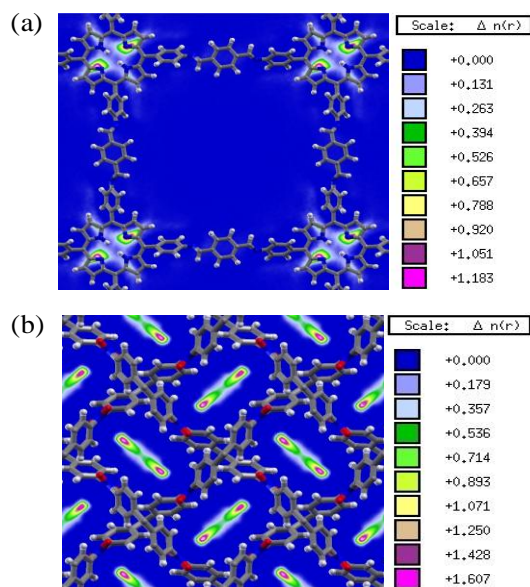
Fig. 4 Contour plots of the COM probability densities of CO_2 from CO_2/N_2 mixture adsorbed in (a) COF-366, (B) NPN-1 at 1 bar (N, blue; O, red; C, gray and H, white).

3.2.3 Structure-sorbent selection parameter relationships

As indicated by eq. 3, the sorbent selection parameter is defined as a product of two terms, which could provide more useful information about the overall separation efficiency for a cyclic PSA or VSA process. The first term was adopted from the "Adsorption Figure of Merit (AFM)",[50] while the second one is the working capacity selectivity taken from the work of Rege and Yang,[51] where the addition of the working capacity of the less strongly adsorbed component in the nominator serves to increase the sensitivity of the dimensionless S_{sp} parameter. In addition, Rege and Yang claimed that pure component isotherms can be sufficient to make a facile calculation of this parameter. However, Ozturk and Keskin[52] recently found the S_{sp} values calculated from mixture adsorption isotherms are higher than the ones predicted from pure component data. This was attributed to the fact that more strongly adsorbed component decreases the adsorption of other less strongly components in the mixtures.

Hence, the S_{sp} values for CO_2/N_2 separation in all the 46 COFs were evaluated using the simulated mixture adsorption data. Considering that both selectivity and working capacity correlate well with ΔAD (Figs. 2 and 3), we directly explored the relationship between this parameter and the sorbent selection parameter of the COFs. The results shown in Fig. 5 demonstrate that S_{sp} is also in good connection with the difference of the adsorbility of adsorbates. It seems that the optimal S_{sp} for COFs in VSA process also appears concentratrely in the region of $1/\Delta AD$ lower than 0.05 (that is, ΔAD larger than 20).

By comparing the simulated S_{sp} values, it was found that some COFs show much better performance than the MOFs studied under the same conditions, such as PCN-26 (38), PCN-9(Co) (120) and PCN-9(Mn) (581).[52] The S_{sp} of these COFs is also much higher than experimentally derived values for the porous organic polymer SNU-C1-va (262),[53] ZIF-78 (396) and the conventional adsorbents such as zeolites 5A (163) and 13X (128).[46] It should be pointed out that the calculations for the latter four materials were conducted for the gas mixture with a bulk composition of $CO_2:N_2=10:90$, on the basis of the ideal adsorbed solution theory with the experimental adsorption isotherms of single gases as input [46,53,]
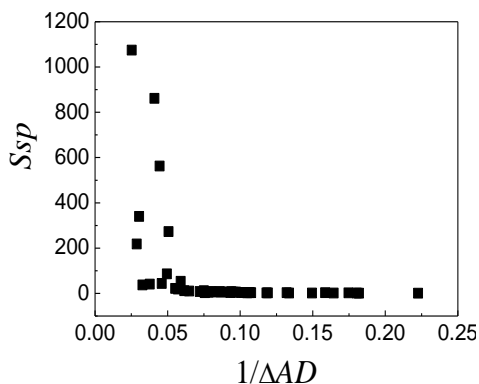
Fig. 5 Relationship between the sorbent selection parameter and ΔAD for CO_2/N_2 separation in the 46 COFs at 298 K using VSA process.

3.3 Evaluation of the Rgenerability of COFs

Regenerability (R) is also an important factor to evaluate a material for practical use. Therefore, the regenerability of the 46 COFs for CO_2 capture was further examined. The results shown in Fig. 6 indicate that all the materials have a regenerability higher than 70% with 42 COFs between 80~90%. Table S48 lists the top 4 COFs in terms of selectivity, working capacity and sorbent selection parameter (see the ESI†). It can be found that they all show a regenerability higher than 85%. Since these top materials are mainly constructed by organic groups with light elements, there are no ultra-strong CO_2 adsorption sites in their structures. Thus, CO_2 molecules interact moderately with these COFs and the highest Q_{st}^0 is ~36 kJ mol^{-1} in TpPa-1, which is much lower than that in the MOFs with open metal sites such as MIL-100(Cr) (63 kJ mol^{-1}).[54] This not only indicates a strong but still reversible adsorption–desorption process in these top materials,[20,55] but also the materials can be potentially regenerated under milder conditions. Furthermore, the regenerability of these COFs is also higher than PCN-26 (72%), PCN-9(Co) (43%) and PCN-9(Mn) (27%)[52] as well as zeolites 5A (67%) and 13X (54%).[46] Therefore, COFs can be considered as promising candidates for CO_2 capture from postcombustion gas with both good separation performance and high regenerability.

From the above analyses, it could be concluded that the three evaluation criteria (adsorption selectivity, CO_2 working capacity and sorbent selection parameter) used for describing the separation performance of COFs correlate strongly with the difference of the adsorbility of adsorbates. Attention can be focused on choosing COFs with a feature of large ΔAD for efficient CO_2/N_2 separation *via* VSA process. More than that, COFs also show a high regenerability in selective adsorption of CO_2, which is favourable for their practical applications.
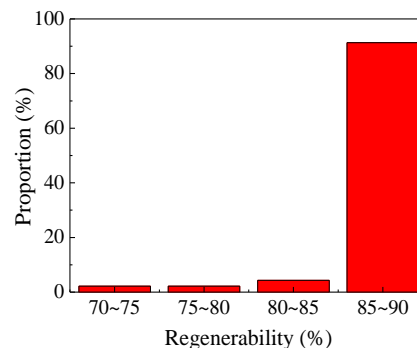
Fig. 6 Distribution of regeneration performance of the 46 COFs.

3.4 Strategy for enhancing separation performance of COFs

The above results demonstrate that parameter ΔAD can serve as a criterion for designing COFs with improved CO_2 capture capability. Generally speaking, two common methods can be utilized to increase the ΔAD for adsorbents:

(i) Chemical modification by introducing polar functional groups into the structure, inducing an increase in ΔQ_{st}^0, in the meantime a reduction in porosity usually. On the other hand, incorporating coordinatively unsaturated metal sites is also an alternative.

(ii) Structural realignment by introducing interpenetration (catenation) in the structure. This method can increase ΔAD *via* generating additional small pores without changing the chemical composition of a material, which will also reduce the porosity to a certain extent normally.
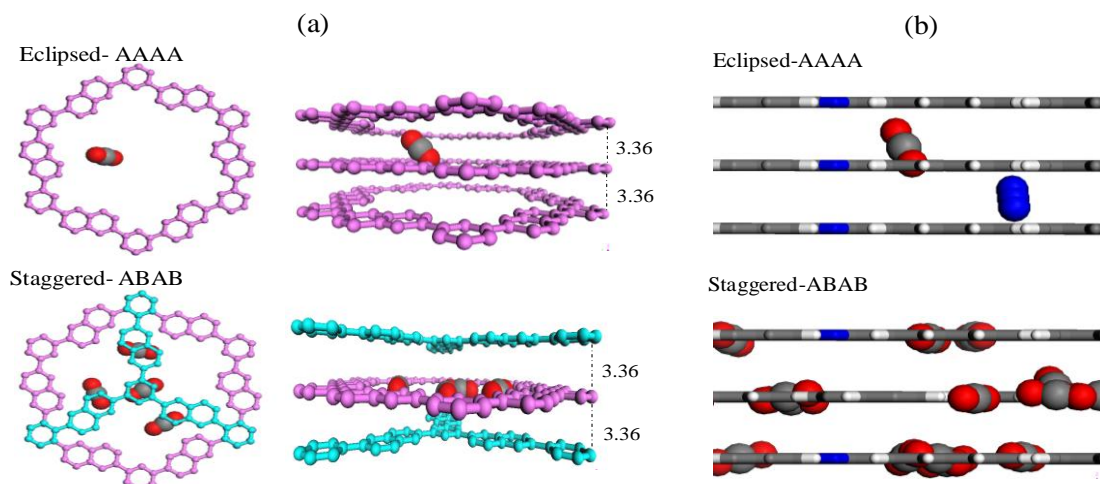
Fig. 7 Snapshots for CO_2/N_2 mixture adsorbed in eclipsed and staggered CTF-2 at 298 K and 1 bar. (a) Views with only CO_2 molecules (left: top view; right: side view; H atoms are omitted for clarity), and (b) mixture cases.

Through analyzing the structural influences of the 46 COFs on CO_2/N_2 separation, we found that there are 12 COFs (4 COFs with 3D-interpenetration structures and 8 materials with 2D-layered ones) on the top level of adsorption selectivity, CO_2 working capacity and sorbent selection parameter. Among the eight 2D-layered COFs, 4 of them (TpPa-1, TpBD, DAAQ-TFP COF and COF-43) show good separation performance due to the presence of special adsorption sites, while for the other 4 COFs (COF-1,[12] COF-366, IL-COF-1 and staggered CTF-2[56]) are resulted from the "right" stacking modes of their layered structures. Previous studies on MOFs have proved, both experimentally and computationally, that framework interpenetration can be employed to improve separation performance.[57-60] For 3D-COFs, Babarao et al.[61] also computationally confirmed that the interpenetrating structures show greatly improved performance for CO_2/N_2 separation compared to the non-interpenetrated counterparts. The strategy of chemical modifications for porous materials has also been studied extensively and is considered as an effective means to enhance the separation properties of materials.[62-65] However, to the best of our knowledge; no study has been conducted so far to investigate the effects of structural stacking modes of 2D-COFs on mixture separation. As a result, in the following we focus on exploring the influences of structural characteristics of the 2D-layered COFs, *i.e.,* the stacking modes of eclipsed AA and staggered AB, on CO_2/N_2 separation. For this purpose, the above four 2D-COFs with the "right" stacking modes were selected as examples for the subsequent detailed analysis.

For CTF-2, our simulation results show that the separation performance of its AB-stacking (staggered) form is much better than the AA-stacking (eclipsed) counterpart. As can be observed from the snapshots shown in Fig. 7, CO_2 molecules are adsorbed in the regular channel pores of eclipsed CTF-2 (denoted as CTF-2-AA) with random spatial orientation. For the case of staggered CTF-2 (denoted as CTF-2-AB), the distance between two consecutive A (B) layers in the structure is ~6.72 Å, and CO_2 molecules are orderly adsorbed in the slit-like pores formed by the staggered layers. Obviously, there are much more CO_2

molecules adsorbed in CTF-2-AB than that in CTF-2-AA. Interestingly, almost all the adsorbed CO_2 molecules in CTF-2-AB are located in the middle position of the slit-like pores, i.e., the B layer between ABA or A layer between BAB. Through this way, CO_2 molecules interact with the A (B) layers in both sides with a distance of ~3.36 Å and one B (A) layer where they sit. Such a phenomenon can also be found in COF-1. In addition, compared to CTF-2-AA which has a ΔAD of 9.3, CTF-2-AB has a much larger value of 24.4, and thus the S_{CO_2/N_2}, ΔN_{CO_2} and S_{sp} are increased by factors of 15, 37 and 281 respectively, with negligible loss of the regenerabilty (changing from 89% to 85%).

In regard to IL-COF-1, the pyrene building units have a planar configuration, but the organic linkers are not coplanar with them (see Fig. 8), thus its structural feature is different from that of CTF-2. For eclipsed IL-COF-1 (IL-COF-1-AA), the snapshots shown in Fig. 8a indicate that the pore spaces formed by the pyrene units in the adjacent layers are the main adsorption sites for CO_2. Since the pyrene units are oriented in an eclipsed conformation, slit-like pores are formed with a width of ~6.57 Å, which provide suitable room for attracting CO_2 molecules. For comparison, we also studied the adsorption behaviour of CO_2/N_2 mixture in the hypothetical staggered counterpart (IL-COF-1-AB) (the structure was constructed from the data in literature,[18] while only the eclipsed form is experimentally synthesized at the moment). In this staggered form, the pyrene units between adjacent layers become staggered and the distance turns out to be 12.54 Å between two consecutively eclipsed pyrene units. As shown in Fig. 8a, the number of CO_2 molecules adsorbed in IL-COF-1-AB is significantly reduced compared to that in IL-COF-1-AA. This can be ascribed to the overlarge stacking distance between two consecutively eclipsed pyrene units, causing a weaker "splint effects". These microscopic origins result in the ΔAD of IL-COF-1-AB 3.5 times lower than that of IL-COF-1-AA, which eventually leads to a worse separation performance in the former.

Similar to IL-COF-1-AA, the organic linkers are also not coplanar with the planar porphyrin building units in the structure of eclipsed COF-366 (denoted as COF-366-AA) and there are
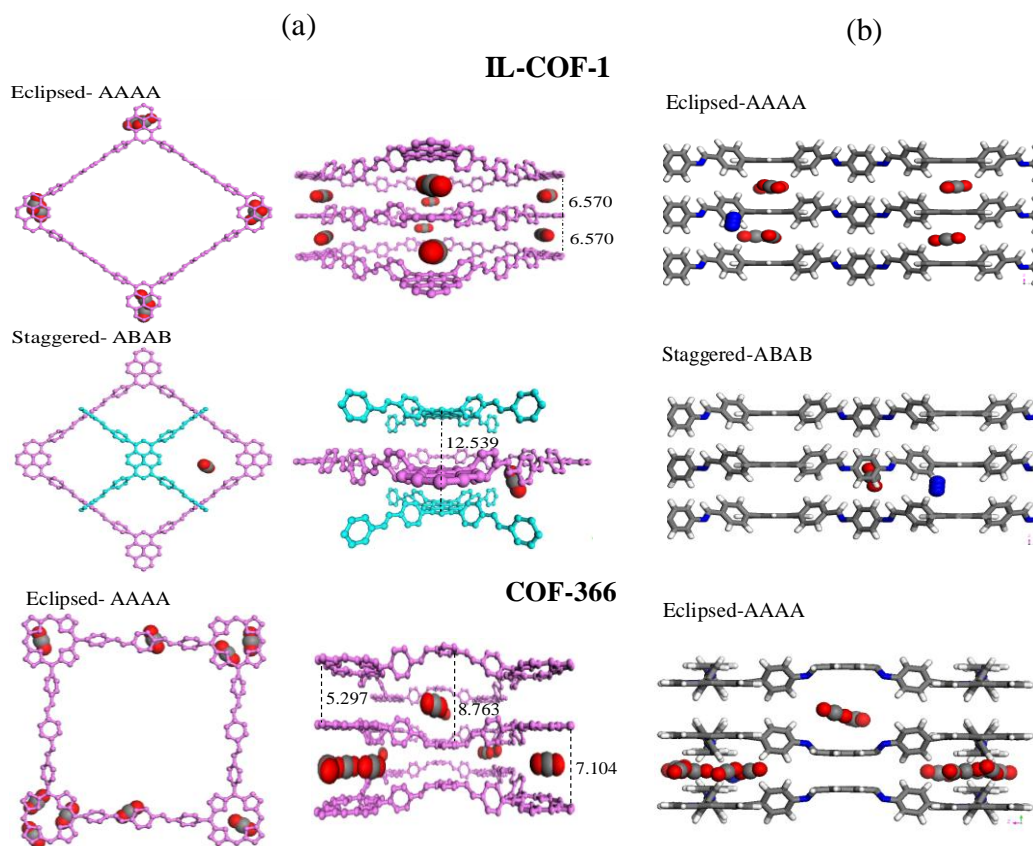
Fig. 8 Snapshots for CO_2/N_2 mixtures adsorbed in IL-COF-1-AA/AB and COF-366-AA at 298 K and 1 bar. (a) Views with only CO_2 molecules (left: top view; right: side view; H atoms are omitted for clarity), and (b) mixture cases.

three types of slit-like pore regions, as shown in Fig. 8a. Specifically, regions 1 and 2 are formed by the eclipsed porphyrin rings in the adjacent layers with distances of ~7.104 and ~5.297 Å, respectively; region 3 is formed by the benzene rings in the adjacent layers with a distance of ~8.763 Å. The snapshots given in Fig. 8b show that CO_2 molecules are mainly adsorbed in the centre of region 1, indicating that such regions are the preferential adsorption sites. Interestingly, there are no CO_2 molecules adsorbed in region 2 under the adsorption conditions considered, together with very fewer CO_2 molecules in region 3. The above results clearly demonstrate that appropriate distances between parallel structures are of great importance for CO_2 capture from flue gas.

Previous studies have shown that the electrostatic properties of materials have significant impacts on their adsorption behaviour of CO_2.[66,67] These studies also indicate that electrostatic potential with large gradient and high absolute value would enhance the performance of a material for CO_2/N_2 separation due to the large difference of their quadrupole moments. Therefore, to show the influences of the stacking modes on the ESP distribution of materials, DFT calculations were further performed by taking the eclipsed and staggered structures of CTF-2 as an example. Fig. 9 shows the DFT-derived contour maps of the ESP in planes through the pore centres of the two structures. Obviously, the ESP in eclipsed CTF-2 has a homogenous distribution along its very regular 1D pore channels (Fig. 9a). In contrast, due to the

splint effects, the ESP distribution in the staggered form has a significant change with much larger gradient between each layer (Fig. 9b), explaining the observations that more CO_2 molecules are attracted in the latter (Fig. 7b) from another point of view.
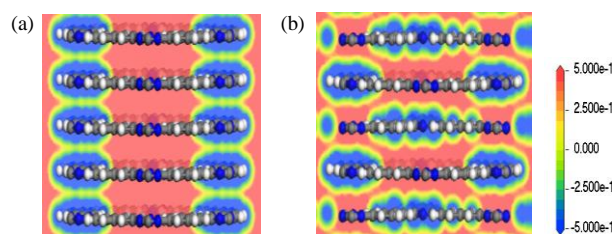
Fig. 9 The contour maps of electrostatic potential (ESP) in planes through the pore centres of (a) eclipsed CTF-2, (b) staggered CTF-2 (N, blue; C, gray, H, white).

3.5 Regulating the separation performance of COFs using the proposed strategy

With the above analysis, it can be concluded that tailoring proper stacking modes to form slit-like pores with appropriate distance can greatly increase the separation performance of 2D-layered COFs for CO_2 capture. To further verify this, Table 1 shows a comparison of the four evaluation criteria for the hypothetical staggered (AB) and the existing eclipsed (AA) structures of three COFs. As can be seen from this table, COF-42-AB,[21] BLP-2H-AB[68] and IL-COF-1-AA all have slit-like pores to impose splint

effects, leading to significant enhancement on the selectivity, CO_2 working capacity and sorbent selection parameter, with only slight decrease in regenerability.

Table 1 Comparison of the four evaluation criteria for the eclipsed (AA) and staggered (AB) structures of three COFs

Materials	COF-42 (AA/AB)	BLP-2H (AA/AB)	IL-COF-1 (AA/AB)
φ	0.72/0.65	0.51/0.50	0.82/0.82
ΔAD	12.5/26.5	10.3/22.6	30.5/6.8
S	7.0/73	6.0/43	23/2.1
ΔN_{CO_2} (mol kg^{-1})	0.18/2.26	0.12/1.50	0.85/0.19
S_{sp}	8.0/875	6.0/235	37/3.1
R (%)	90/88	90/85	78/90

It is worth noting that the proper stacking distance between layers is important to produce strong splint effects on CO_2 adsorption. To further make this clear, CTF-2 in staggered form was selected as an example to finely tune the stacking distance between adjacent layers, due to its very simple structure with slit-like pores. The stacking distance between adjacent layers was artificially adjusted to 5, 6, 7 and 8 Å, respectively. The calculations show that the resulting CO_2/N_2 adsorption selectivities are 3, 65, 41 and 12, respectively. Actually, similar observations have also been found for other 2D-layered COFs with slit-like pores. These examples confirm that the separation performance of 2D-layered COFs can be greatly enhanced by generating "splint effects", which can be achieved through structural realignment to form slit-like pores with suitable size.

4. Conclusion

The multi-scale computations based on the database containing 46 typical COFs with broad chemical and topological diversities show that adsorption selectivity, CO_2 working capacity and sorbent selection parameter are highly correlated with the difference of adsorbility (ΔAD) between CO_2 and N_2, and most of the COFs exhibit high regenerability. The results indicate that ΔAD is a good indicator for the separation performance of COFs for CO_2 capture, which may serve as a criterion for rational design of new COFs. In addition, this work found that introducing slit-like pores with suitable size to exert "splint effects" on CO_2 adsorption is a good strategy to design COFs for CO_2 capture, which can be realized by structural realignment of 2D-COFs, similar to the "catenation effects" in 3D-COFs formed by interpenetration. The microscopic information and knowledge obtained in this work will contribute to a better understanding of the structure-property relationships of COFs for CO_2 capture, and thus guiding the future rational design of new COFs, which is also applicable to other porous materials and gas separation processes related to the fields of energy and environmental science and technology.

Acknowledgements

Notes and references

State Key Laboratory of Organic-Inorganic Composites, Beijing University of Chemical Technology, Beijing 100029, China;
E-mail: zhongcl@mail.buct.edu.cn, qyyang@mail.buct.edu.cn
† Electronic Supplementary Information (ESI) available: Structural details of the COFs, LJ parameters, model clusters and atomic partial charges, and some additional results. See DOI:10.1039/b000000x/

1. J.-R. Li, J. Sculley and H.-C. Zhou, *Chem. Rev.*, 2012, **112**, 869−932.
2. D. M. D'Alessandro, B. Smit, J. R. Long, *Angew. Chem., Int. Ed.*, 2010, **49**, 6058−6082.
3. G. Férey, C. Serre, T. Devic, G. Maurin, H. Jobic, P. L. Llwewllyn, G. De Weireld, A. Vimont, M. Daturi and J.-S. Chang, *Chem. Soc. Rev.*, 2011, **40**, 550−562.
4. R. Krishna and J. M. van Baten, *Phys. Chem. Chem. Phys.*, 2011, **13**, 10593−10616.
5. S. T. Meek, J. A. Greathouse and M. D. Allendorf, *Adv. Mater.*, 2011, **23**, 249−267.
6. T.-H. Bae, M. R. Hudson, J. A. Mason, W. L. Queen, J. J. Dutton, K. Sumida, K. J. Micklash, S. S. Kaye, C. M. Brown and J. R. Long, *Energy Environ. Sci.*, 2013, **6**, 128−138.
7. J. Jiang, R. Babarao and Z. Hu, *Chem. Soc. Rev.*, 2011, **40**, 3599−3612.
8. E. Haldoupis, S. Nair and D. S. Sholl, *J. Am. Chem. Soc.*, 2012, **134**, 4313−4323.
9. L.-C. Lin, A. H. Berger, R. L. Martin, J. Kim, J. A. Swisher, K. Jariwala, C. H. Rycroft, A. S. Bhown, M. W. Deem, M. Haranczyk and B. Smit, *Nat. Mater.*, 2012, **11**, 633−641.
10. D. Wu, Q. Yang, C. Zhong, D. Liu, H. Huang, W. Zhang and G. Maurin, *Langmuir*, 2012, **28**, 12094−12099.
11. C. E. Wilmer, O. K. Farha, Y.-S. Bae, J. T. Hupp and R. Q. Snurr, *Energy Environ. Sci.*, 2012, **5**, 9849−9856.
12. A. P. Côté, A. I. Benin, N. W. Ockwig, M. O'Keeffe, A. J. Matzger and O. M. Yaghi, *Science*, 2005, **310**, 1166−1170.
13. S.-Y. Ding and W. Wang, *Chem. Soc. Rev.*, 2013, **42**, 548−568.
14. X. Feng, X. Ding and D. Jiang, *Chem. Soc. Rev.*, 2012, **41**, 6010–6022.
15. Z. Chang, D.-S. Zhang, Q. Chen and X.-H. Bu, *Phys. Chem. Chem. Phys.*, 2013, **15**, 5430−5442.
16. E. Tylianakis, E. Klontzasa and G. E. Froudakis, *Nanoscale*, 2011, **3**, 856–869.
17. H. Furukawa and O. M. Yaghi, *J. Am. Chem. Soc.*, 2009, **131**, 8875−8883.
18. M. G. Rabbani, A. K. Sekizkardes, Z. Kahveci, T. E. Reich, R. Ding and H. M. El-Kaderi, *Chem. Eur. J.*, 2013, **19**, 3324−3328.
19. A. Bhunia, I. Boldog, A. Möller and C. Janiak, *J. Mater. Chem. A*, 2013, **1**, 14990−14999.
20. Y. Zhao, K. X. Yao, B.Teng, T. Zhang and Y. Han, *Energy Environ. Sci.*, 2013, **6**, 3684−3692.
21. F. J. Uribe-Romo, C. J. Doonan, H. Furukawa, K. Oisaki and O. M. Yaghi, *J. Am. Chem. Soc.*, 2011, **133**, 11478−11481.
22. S. Kandambeth, A. Mallick, B. Lukose, M. V. Mane, T. Heine, and R. Banerjee, *J. Am. Chem. Soc.*, 2012, **134**, 19524−19527.
23. B. P. Biswal, S. Chandra, S. Kandambeth, B. Lukose, T. Heine and R. Banerjee, *J. Am. Chem. Soc.*, 2013, **135**, 5328−5331.
24. S. Chandra, S. Kandambeth, B. P. Biswal, B. Lukose, S. M. Kunjir, M. Chaudhary, R. Babarao, T. Heine, and R. Banerjee, *J. Am. Chem. Soc.*, 2013, **135**, 17853−17861.
25. C. R. DeBlase, K. E. Silberstein, T.-T. Truong, H. D. Abruña and W. R. Dichtel, Energy Storage, *J. Am. Chem. Soc.*, 2013, **135**, 16821−16824.
26. X. Feng, Y. Dong and D. Jiang, *CrystEngComm*, 2013, **15**, 1508−1511.
27. P. Kuhn, M. Antonietti and A. Thomas, *Angew. Chem., Int. Ed.*, 2008, **47**, 3450−3453.
28. D. Beaudoin, T. Maris and J. D. Wuest, *Nat., Chem.*, 2013, **5**, 830−834.
29. S. Amirjalayer, R. Q. Snurr and R. Schmid, *J. Phys. Chem. C*, 2012, **116**, 4921-4929.
30. V. Mulgundmath and F. H. Tezel, *Adsorption*, 2010, **16**, 587−598.

31. M. M. Francl, C. Carey, L. E. Chirlian and D. M. Gange, *J. Comput. Chem.*,1996, **17**, 367−383.

32. R. Babarao and J. Jiang, *Energy Environ. Sci.*, 2008, **1**, 139−143.

33. H. Heinz and U. W. Suter, *J. Phys. Chem. B*, 2004, **108**, 18341−18352.

34. M. J. Frisch, G. W. Trucks and H. B. Schlegel, GAUSSIAN 03, Rev. B.1; Gaussian, Inc.: Pittsburgh, PA, 2003.

35. Q. Yang, D. Liu, C. Zhong and J.-R. Li, *Chem. Rev.*, 2013, **113**, 8261−8323.

36. C. Zheng and C. Zhong, *J. Phys. Chem. C*, 2010, **114**, 9945−9951.

37. Y. Liu, D. Liu, Q. Yang, C. Zhong and J. Mi, *Ind. Eng. Chem. Res.*,2010, **49**, 2902−2906.

38. Accelrys Inc., Materials Studio, V5.0, Accelrys Inc., San Diego, CA, 2003.

39. J. Lan, D. Cao and W. Wang, *Langmuir,* 2010, **26**, 220−226.

40. J. G. Harris and K. H. Yung, *J. Phys. Chem.*, 1995, **99**, 12021−12024.

41. J. J. Potoff, and J. I. Siepmann, *AIChE J.*, 2001, **47**, 1676−1682 .

42. S. L. Mayo, B. D. Olafson and W. A. Goddard III, *J. Phys. Chem.*, 1990, **94**, 8897−8909.

43. A. K. Rappé, C. J. Casewit, K. S. Colwell, W. A. Goddard III, W. M. Skiff, *J. Am. Chem. Soc.*, 1992, **114**, 10024−10039.

44. S. Keskin, *J. Phys. Chem. C*, 2012, **116**, 1772−1779.

45. T. J. H. Vlugt, E. García-Pérez, D. Dubbeldam, S. Ban and Calero,S, *J. Chem. Theory Comput.*, 2008, **4**, 1107−1118.

46. Y.-S. Bae and R. Q. Snurr, *Angew. Chem., Int. Ed.*, 2011, **50**, 11586−11596.

47. D. Wu, C. Wang, B. Liu, D. Liu, Q. Yang and C. Zhong, *AIChE J.*, 2012, **58**, 2078−2084.

48. K.E. Hart, L. J. Abbott, N. B. McKeown and C. M. Colina, *Macromolecules*, 2013, **46**, 5371−5380.

49. S. Wan, F. Gandara, A. Asano, H. Furukawa, A. Saeki, S. K. Dey, L. Liao, M. W. Ambrogio, Y. Y. Botros, X. Duan, S. Seki, J. F. Stoddart and O. M. Yaghi, *Chem. Mater.*, 2011, **23**, 4094−4097.

50. F. Notaro, J. T. Mullhaupt, F. W. Leavitt, M. W. Ackley and Praxair, US Patent 5, 810,909,1998.

51 S. U. Rege and R. T. Yang, *Sep. Sci. Technol.*, 2001, **36**, 3355−3365.

52. T. N. Ozturk and S. Keskin, *Ind. Eng. Chem. Res.*, 2013, **52**, 17627−17639.

53. L.-H. Xie and M.P. Suh, *Chem. Eur. J.*, 2013,**19**,11590−11597.

54. P. L. Llewellyn, S. Bourrelly, C. Serre, A. Vimont, M. Daturi, L. Hamon, G. De Weireld, J. S. Chang, D. Y. Hong, Y. K. Hwang, S. H. Jhung and G Férey, *Langmuir*, 2008, **24**, 7245−7250.

55. P. Nugent, Y. Belmabkhout, S. D. Burd, A. J. Cairns, R. Luebke, K. Forrest, T. Pham, S. Ma, B. Space, L. Wojtas, M. Eddaoudi and Michael J. Zaworotko, *Nature*, 2013, **7**, 495, 80−84.

56. M. J. Bojdys, J. Jeromenok, A. Thomas and M. Antonietti, *Adv. Mater.*, 2010, **22**, 2202−2205.

57. D. Frahm, M. Fischer, F. Hoffmann and M. Fröba, *Inorg. Chem.*, 2011, **50**, 11055−11063.

58. J. Park, J.-R. Li, Y.-P. Chen, J. Yu, A. A. Yakovenko, Z. U. Wang, L.-B. Sun, P. B. Balbuena and H.-C. Zhou, *Chem. Commun.*, 2012, **48**, 9995−9997.

59. S. Yang, X. Lin, W. Lewis, M. Suyetin, E. Bichoutskaia, J. E. Parker, C. C. Tang, D. R. Allan, P. J. Rizkallah, P. Hubberstey, N. R. Champness, K. M. Thomas, A. J. Blake and M. Schroeder, *Nat. Mater.*, 2012, **11**, 710−716.

60. R. Babarao, J. W. Jiang, and S. I. Sandler, *Langmuir*, 2009, **25**, 5239−5247.

61. R. Babarao, R. Custelcean, B.P. Hay and D. Jiang, *Cryst. Growth Des.*, 2012, **12**, 5349−5356.

62. C. Montoro, E. García, S. Calero, M. A. Pérez-Fernández, A. L. López, E. Barea and J. A. R. Navarro, *J. Mater. Chem.*, 2012, **22**, 10155−10158.

63. J. J. Williams, A. D. Wiersum, N. A. Seaton and T. Düren, *J. Phys. Chem. C*, 2010, **114**, 18538−18547.

64. A. F. Combariza and G. Sastre, *J. Phys. Chem. C*, 2011, **115**, 13751−13758.

65. Q. Yang, S. Vaesen, F. Ragon, A. D. Wiersum, D. Wu, A. Lago, T. Devic, C. Martineau, F. Taulelle, P. L. Llewellyn, H. Jobic, C.Zhong, C. Serre, G. D. Weireld and G. Maurin, *Angew. Chem., Int. Ed.*, 2013, **52**, 10316−10320.

66. Q. Yang and C.Zhong, *ChemPhysChem*, 2006, **7**, 1417−1421.

67. Z. Zhang, Z. Li, and J. Li, *Langmuir*, 2012, **28**, 12122−12133.

68. K. T. Jackson, T. E. Reich and H. M. El-Kaderi, *Chem. Commun.*, 2012, **48**, 8823−8825.